



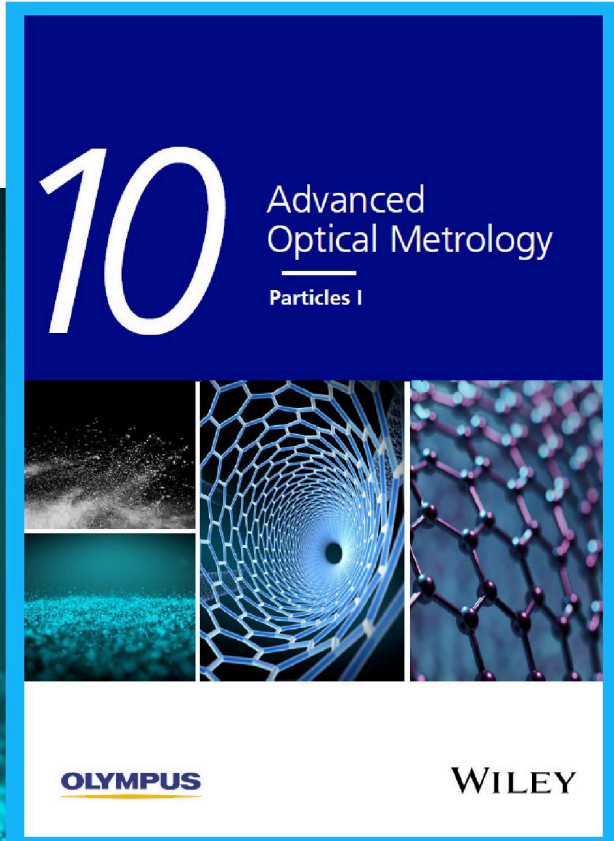
Particles I

Access the latest eBook →

Particles: Unique Properties,
Uncountable Applications

Read the latest eBook and
better your knowledge with
highlights from the recent
studies on the design and
characterization of micro-
and nanoparticles for
different application areas.

[Access Now](#)



This eBook is sponsored by

OLYMPUS[®]

WILEY

Cell Membrane-Inspired Graphene Nanomesh Membrane for Fast Separation of Oil-in-Water Emulsions

Yanan Liu* and Marc-Olivier Coppens*

Graphene exhibits fascinating prospects for preparing high-performance membranes with fast water transport, due to its low friction with water and extreme thinness. However, for graphene-assembled membranes, each molecule passing through the membrane should bypass many graphene sheets, which lengthens the molecular pathways and increases the mass transfer resistance. Herein, a graphene nanomesh (GNM) membrane is fabricated that is inspired by cell membranes, including aquaporins with their hydrophilic gate for selective transport and hydrophobic channel for low friction with water, thus resulting in fast water transport, as well as hydrophilic polymer brushes on the membrane surface for fouling resistance. GNM is synthesized by etching nanopores on graphene oxide (GO) nanosheets to significantly shorten the water transport channels, whereas the hydrophobic graphene sheets lead to low water friction; in combination, ultra-fast, selective water flux is achieved. Also, hydrophilic polymer chitosan is utilized to modify GNM to construct a hydration layer, which suppresses foulants from touching the membrane surface. Accordingly, the permeance of the cell membrane-inspired graphene nanomesh membrane reaches almost $4000 \text{ L m}^{-2} \text{ h}^{-1} \text{ bar}^{-1}$, which is about 260 times the permeance in a GO membrane, and the membranes show superior antifouling properties for separating various surfactant-stabilized oil-in-water emulsions.

clean water; as a result, significant fresh water shortages have become commonplace.^[1–3] Oil-containing wastewater has turned into a major environmental concern in daily life and for a large number of industries, such as food, leather, textile, steelmaking, petrochemical and metal finishing industries, as the direct discharge of it is harmful to human health and the environment.^[4–6] Compared with the traditional water treatment technologies, membrane technology presents a lot of advantages, including highly selective separation, low energy consumption, easy equipment and low space needs, as well as continuous and automatic operation, especially for the separation of emulsified oil/water mixtures.^[7,8] The separation of such emulsified oil/water mixtures is challenging when using traditional techniques, such as centrifuges, coalescers and oil skimmers, especially as they lose their separation efficiency when the oil droplet size is below $20 \mu\text{m}$.^[9–11]

Graphene oxide (GO), with its two-dimensional (2D) carbon structure and single carbon atom thickness, has become

a popular membrane material, on account of its unique features, such as excellent mechanical strength, high surface area and flexibility, low friction with water and gas, as well as the possibility of large-scale production.^[12–17] After the first work on GO-based membranes was reported in 2007,^[18] many more studies followed, including GO-blended membranes with the potential of large-scale production and aminated GO-based membranes with the ability of precise separation.^[19–25] The super-thin 2D structure of nanosheets is of great benefit to assemble the individual GO layers into a laminated GO-based membrane by interlayer interactions, such as hydration bonds, π - π interactions and van der Waals interactions.^[14,26–28] The laminated channels provide passageways for transport and separation, which could be effectively adjusted by different methods, like partial reduction, cross-linking and physical confinement.^[29–35]


In existing GO-based membranes, most attention is paid to controlling the interlayer spacing for different separation purposes through intercalating ions, molecules or nanomaterials between adjacent GO nanosheets, because the interlayer spacing plays a key role in determining the separation properties of GO-based membranes, like the pore size of traditional membranes, which allows desired species to pass through and

1. Introduction

Industrialization and population growth have led to increasing urbanization globally, in addition to rising requirement for

Y. Liu, M.-O. Coppens
Department of Chemical Engineering
Centre for Nature-Inspired Engineering
University College London
London WC1E 7JE, UK
E-mail: m.coppens@ucl.ac.uk

Y. Liu
School of Chemical Engineering and Technology
Hainan University
Haikou 570228, China
E-mail: liuyan@hainanu.edu.cn

 The ORCID identification number(s) for the author(s) of this article can be found under <https://doi.org/10.1002/adfm.202200199>.

© 2022 The Authors. Advanced Functional Materials published by Wiley-VCH GmbH. This is an open access article under the terms of the Creative Commons Attribution License, which permits use, distribution and reproduction in any medium, provided the original work is properly cited.

DOI: 10.1002/adfm.202200199

rejects unwanted species.^[36–40] Limitations of this approach are the precision with which the interlayer spacing can be controlled, the stability of the interlayer spacing in water and the high mass transfer resistance arising from the long mass transfer channels. Indeed, molecules passing through a graphene-based membrane should bypass graphene nanosheets, which lengthen the mass transfer channel and enlarge the mass transfer resistance, thus decreasing the membrane permeance.

The cell membrane, a biological membrane consisting of a lipid bilayer, proteins and some hydrophilic polymer brushes, is a barrier that separates the cell's interior from the outside environment to protect the cell and control the flux of ions and molecules in and out of the cell.^[41] Arguably, aquaporins are the most important membrane proteins that go across the cell membrane, as they have the ability to efficiently regulate water, ions and other solutes through the cell membrane. This is due to the hydrophobic channel and minimal number of water binding sites in aquaporins to facilitate rapid water transport, as well as steric effects and ion binding sites to control the transport of ions and molecular solutes.^[42,43] Meanwhile, the hydrophilic polymer brushes outside the cell membrane can serve as a protector through steric hindrance and by forming a repelling hydration layer on the cell membrane surface.

Herein, inspired by the structure of the cell membrane, a graphene nanomesh membrane was fabricated through a vacuum-assisted self-assembly process. Nanopores were synthesized on graphene nanomesh (GNM)^[44,45] to decrease the length of the mass transfer channels. Combined with the low friction between graphene nanosheets and water molecules, high permeance was realized as a result of low mass transfer resistance. Chitosan with hydrophilic hydroxyl groups and amino groups was used to modify GNM to increase its hydrophilicity and induce the formation of a hydration layer on the membrane surface. Accordingly, the membrane possessed high hydrophilicity, super-oleophobicity and low oil adhesion underwater. Hence, the membrane showed excellent antifouling properties when used to separate various kinds of surfactant-stabilized oil-in-water emulsions.

2. Results and Discussion

2.1. Preparation and Characterization of GNM and CS@GNM

The GNM with nanopores was synthesized in two steps using partial combustion.^[46] Firstly, a salt template was formed on GO nanosheets by filtering a concentrated solution of GO and salt on a filtration paper. After drying, a layer of salt template with defective pores was formed on the surface of the GO nanosheets. Then, after ignition, the exposed, bare GO in the defective pores was burned. Finally, the GNM with nanopores was obtained after washing the salts away with HCl solution (Figure S1, Supporting Information). Transmission electron microscopy (TEM) and atomic force microscopy (AFM) were utilized to measure the morphology of the GNM. As shown in the TEM image (Figure 1a), the as-prepared GNM possesses a nanosheet-like structure with sheet size of 300 nm and the pores are distributed uniformly on the GNM, which are confirmed from AFM images (Figure 1b). By analyzing TEM

images of GNM, the average pore size of GNM was found to be 5.5 ± 2.6 nm, and the porosity was about 6.5%. At the same time, the thickness of the GNM was evaluated by AFM to be about 0.8 nm, demonstrating that the GNM is a single layer.

Chitosan was utilized to modify GNM to fabricate CS@GNM with high hydrophilicity, through the reaction of amino groups on chitosan and carboxyl groups on GNM. After rinsing and drying, Fourier transform infrared spectrometer (FTIR) was used to measure the chemical structures of chitosan, GO, GNM and CS@GNM (Figure 1c). There are obvious peaks at 3000–3500 cm^{-1} in the FTIR spectra of chitosan, CS@GNM, GNM and GO for the stretching vibrations of N–H or O–H. The peaks at 2800–3000 cm^{-1} are formed by the stretching vibrations of CH_2 . The specific absorption peaks at 1722 and 1624 cm^{-1} are related to the stretching vibrations of C=O and C=C, respectively, in GO, GNM and CS@GNM, and the specific peaks at 1550–1650 cm^{-1} are due to the bending vibrations of N–H in chitosan and CS@GNM. Accordingly, the appearance of peaks at 1722, 1624, and 1550–1650 cm^{-1} in FTIR spectra of CS@GNM demonstrates that GNM has been successfully modified by chitosan. Similar conclusions are drawn from the high-resolution XPS spectrum of the N 1s region, based on the presence of a N–C=O peak (Figure S2, Supporting Information). The mass ratio of chitosan to GNM in CS@GNM was measured by thermogravimetric analysis (TGA) within a temperature range of 50–800 °C. As shown in Figure 1d, there are three typical stages of mass loss in the TGA curve of GO, associated to the evaporation of water adsorbed at temperatures of less than 100 °C, the thermal decomposition of unstable oxygen-containing functional groups at a temperature of ≈ 200 °C and the combustion of the carbon skeleton at a temperature of ≈ 500 °C. Because the oxygen-containing functional groups in GO were consumed during the process of fabricating the nanopores on GNM, the GNM showed less mass loss than GO at a temperature of ≈ 200 °C. Meanwhile, chitosan exhibited a continuous mass loss within a temperature range of 220–580 °C, resulting from molecular decomposition. CS@GNM possesses a similar TGA curve to GNM at temperatures below 220 °C, but more mass than for GNM is lost when the temperature is above 220 °C, due to the decomposition of chitosan in CS@GNM. Hence, the mass percentage of GNM in CS@GNM could be calculated to be ≈ 87 wt%. The result also demonstrates that GNM was successfully modified by chitosan.

2.2. Preparation and Morphology of the Cell Membrane-Inspired GNM Membrane

The cell membrane-inspired GNM membrane was prepared by a vacuum-assisted self-assembly process, through filtering dispersions of GNM and CS@GNM on the polyether sulfone (PES) membranes with a pore size of 100 nm. Keeping the total mass of GNM and GNM in CS@GNM constant and changing the mass ratio of GNM and GNM in CS@GNM, a series of cell membrane-inspired GNM membranes was fabricated, denoted GNM/CS@GNM- x , with $x = 1$ –6 for mass ratios of $(6-x)$ GNM to x CS@GNM. As shown in Figure 2, the GO membrane possesses a flat surface, due to the flexibility of the GO nanosheets. Also the GNM membrane has a

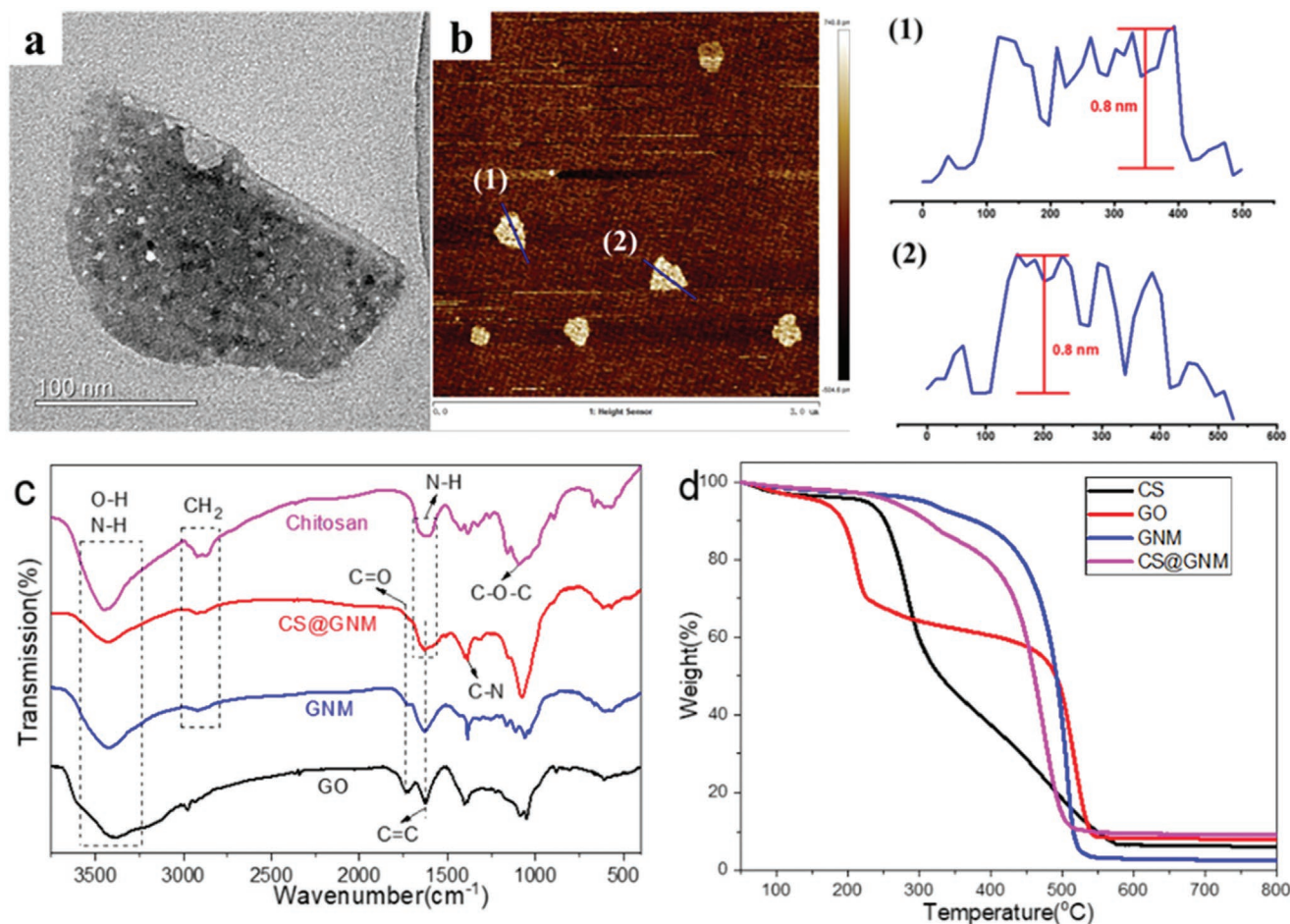


Figure 1. a) TEM and b) AFM images of GNM, c) FTIR spectra, and d) TGA of chitosan, GO, GNM, and CS@GNM.

flat surface, demonstrating that GNM has a similar ability to form a membrane as GO. There are some functional groups on GNM, such as carboxyl groups and hydroxyl groups, and there are amino groups on CS@GNM, because of the unreacted amino groups on chitosan, which is proven by FTIR spectroscopy (Figure 1c). The interactions between amino groups on CS@GNM and carboxyl groups on GNM could bind CS@GNM and GNM together; neighboring GNM could be crosslinked as well.^[47] Accordingly, a well-aligned, layered structure could be produced. With increased fraction of CS@GNM, there was no obvious difference visible at the surface of the cell membrane-inspired GNM. The surface roughness parameter R_a (the mean of the height data) of all the membranes was between 30 and 40 nm, and the roughness parameter R_q (the root mean square of the height data) of all the membranes was between 40 and 50 nm, as shown in Figure S3 (Supporting Information). The thickness of the cell membrane-inspired GNM membrane was also obtained via SEM images of cross-sections of the membranes. The GO membrane exhibited a thickness of 35.7 ± 6.0 nm, and the thickness of the GNM was 42.8 ± 5.3 nm. With increased fraction of CS@GNM, the membrane thickness increased further, because of the increased amount of chitosan in the membranes, up to 80.2 ± 4.3 nm for GNM/CS@GNM-6.

2.3. Wettability of the Cell Membrane-Inspired GNM Membrane

For water treatment membranes, the surface wettability is a crucial factor that influences their fouling behavior. Fouling could be stopped from touching the membrane surface through a hydration layer and steric hindrance. Hence, a series of contact angle measurements were taken to evaluate the surface wettability of the cell membrane-inspired GNM membranes, including dynamic water contact angles in the air and oil contact angles underwater. As shown in **Figure 3**, due to the hydrophilic groups on GO nanosheets, such as hydroxyl groups, carboxyl groups and epoxy groups, the GO membrane exhibited a hydrophilic surface with a water contact angle of $\approx 83^\circ$. At the same time, the water contact angle of GO membranes was kept stable due to the densely packed layered structure. As a comparison, the GNM membrane showed a higher water contact angle and a quicker decline of the water contact angle, because of the consumption of hydrophilic groups during the creation of the nanopores on the GNM, and water permeation was accelerated by the nanopores on GNM. Accordingly, the water contact angle of the GNM membrane was initially about 105° , but it declined to zero in 16.3 s. Thanks to the hydrophilicity of its amino groups and hydroxyl groups, chitosan could be utilized to make the GNM membrane more hydrophilic.

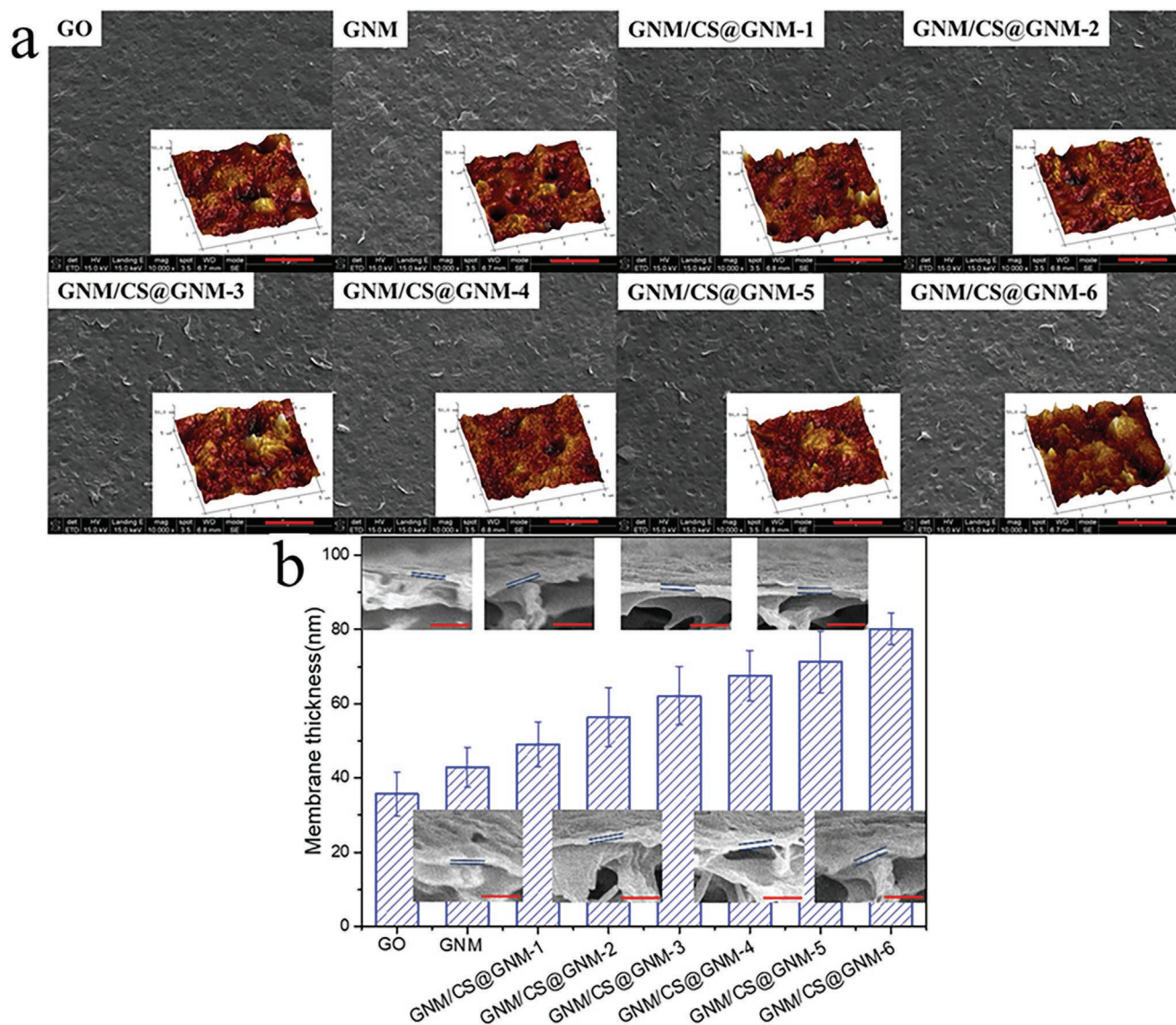


Figure 2. a) SEM and AFM images of the cell membrane-inspired GNM membrane, b) Thickness and SEM images of cross-sections of the cell membrane-inspired GNM membrane; the error bars are based on seven positions measured for each membrane. The scale bar of (a) and (b) represent 5 μm and 500 nm, respectively, and the area of the AFM image is 5 μm \times 5 μm . The blue lines in (b) are used to mark the edges of the membranes.

Therefore, the water contact angles of GNM/CS@GNM- x membranes decreased with increased x , i.e., more CS@GNM in the membrane. Simultaneously, modifying GNM with chitosan could contribute to a decrease in pore size on GNM and the formation of a much denser membrane structure. Combined with the improved hydrophilicity, the time for the water contact angle to decrease to zero increased first and then decreased. In consequence, the water contact angle of GNM/CS@GNM-6 could reach 75° and decrease to zero in 176 s, demonstrating that the cell membrane-inspired GNM membrane possessed high hydrophilicity. Moreover, high hydrophilicity improved by chitosan modification could bond water molecules to the interface between water and the membrane, leading to a robust hydration layer on the membrane surface. By improving the hydrophilicity of the membrane surface, the interaction between the membrane surface and the foulants

could be decreased and the water bonded to the membrane surface would form a protective hydration structure to suppress the oil droplets from completely adhering on the membrane surface, resulting in super-oleophobicity underwater. The GO membrane exhibited a high oil contact angle underwater of $\approx 143.7^\circ$ on account of the hydration layer formed by the hydrophilic groups. Compared with the GO membrane, the GNM membrane showed a lower oil contact angle underwater of $\approx 110.7^\circ$, due to the consumption of hydrophilic groups on GNM. With an increase of CS@GNM in the membranes, more water could be trapped on the membrane surface to form a much more robust hydration layer; hence, the oil contact angle underwater could reach up to 159.8° for the GNM/CS@GNM-6 membrane. Meanwhile, the cell membrane-inspired functionalized GNM membranes presented super-oleophobicity underwater for various oils, including sunflower oil, pump oil, octane

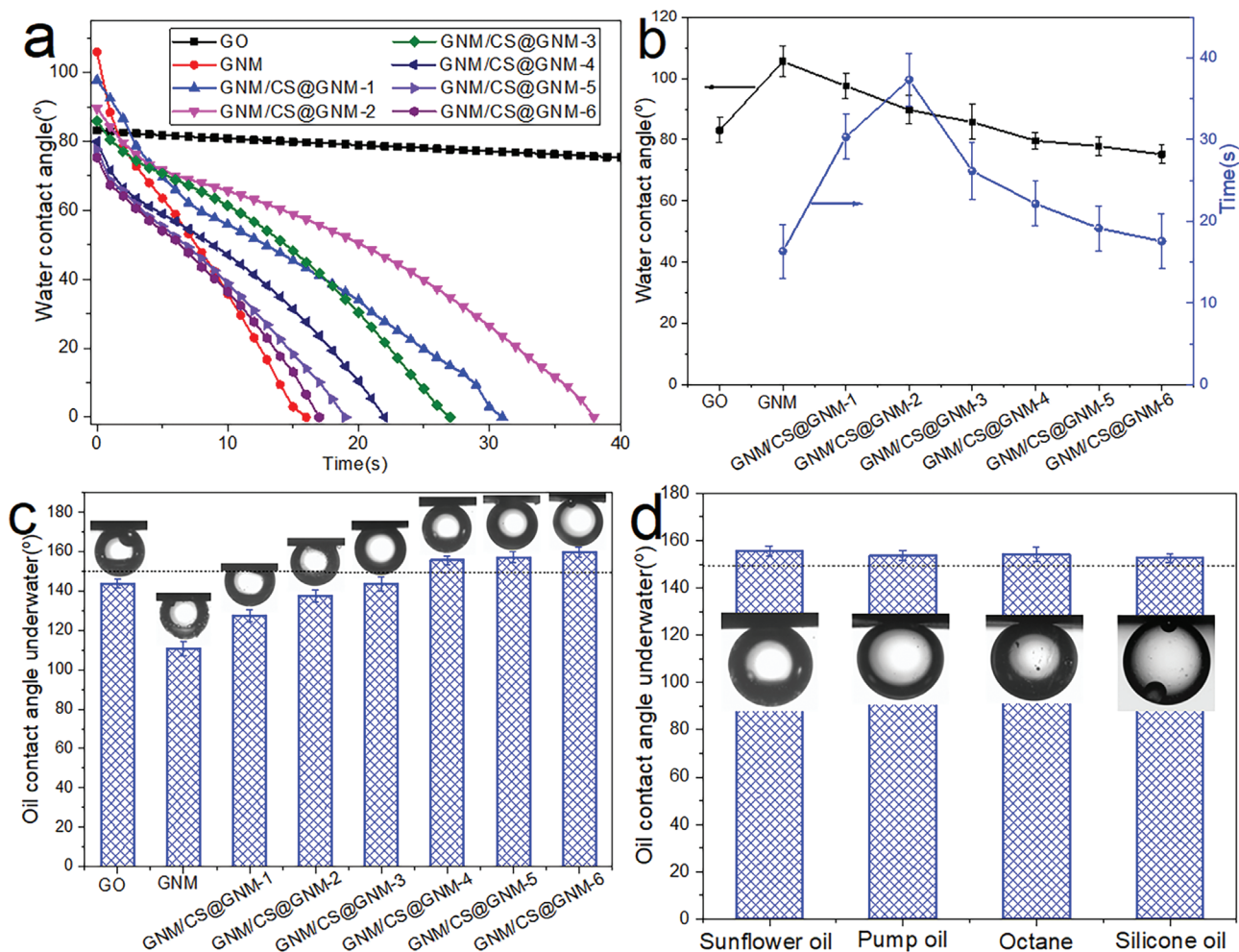


Figure 3. a) The dynamic water contact angle, b) the instantaneous water contact angle and time for the water contact angle to decrease to 0°, c) Sunflower oil contact angles underwater, and d) the oil contact angles for different oils underwater of the cell membrane-inspired GNM/CS@GNM-6 membrane. Error bars are based on seven positions measured for each membrane.

and silicone oil (Figure 3). In addition, a dynamic oil adhesion process, including an oil drop approach, compression and detachment was conducted to measure the adhesion force of the oil droplet and the membrane surface underwater, demonstrating a super-low oil adhesion force for the membrane surface (Figure S4, Supporting Information). Hence, the cell membrane-inspired GNM membrane is endowed with high hydrophilicity, super-oleophobicity and low oil adhesion underwater, which favor superior antifouling and stability for long-term operation for wastewater treatment.

2.4. Permeance and Morphological Stability of the Cell Membrane-Inspired GNM Membrane

The Hagen–Poiseuille equation was used to analyze the permeation flux of liquid through the open pores of the membrane. As shown in this equation, $J = \frac{\epsilon \pi r_p^2 \Delta p}{8 \mu \tau L}$, the permeation flux of the membrane is directly proportional to the membrane porosity, ϵ , and inversely proportional to the membrane thickness, L .^[48] The flux is reduced by a factor

τ , due to the tortuosity and constrictions of the channels. Accordingly, increasing membrane porosity and decreasing membrane thickness and channel tortuosity are useful ways to improve membrane permeability. In this work, the nanopores on GNM could offer more mass transfer channels and decrease the average length of the mass transfer channels, leading to a membrane structure with higher porosity and lower tortuosity. Hence, the permeance of the GNM membrane was dramatically enhanced to $3690 \pm 160 \text{ L m}^{-2} \text{ h}^{-1} \text{ bar}^{-1}$, which is 230 times that of the GO membrane. Simultaneously modifying GNM with chitosan could decrease the pore size on GNM and, with increased fraction of CS@GNM in the membrane, the cell membrane-inspired GNM membranes becomes thicker, as shown in Figure 2; these factors are not favorable for the membrane permeance. However, modifying GNM with chitosan increases the hydrophilicity of the membranes, as shown in Figure 3, which benefits the membrane permeance. As a result, when the fraction of CS@GNM in the membranes increases, the permeance of the cell membrane-inspired GNM membrane first increases, and then decreases, as shown in Figure 4a and Table 1.

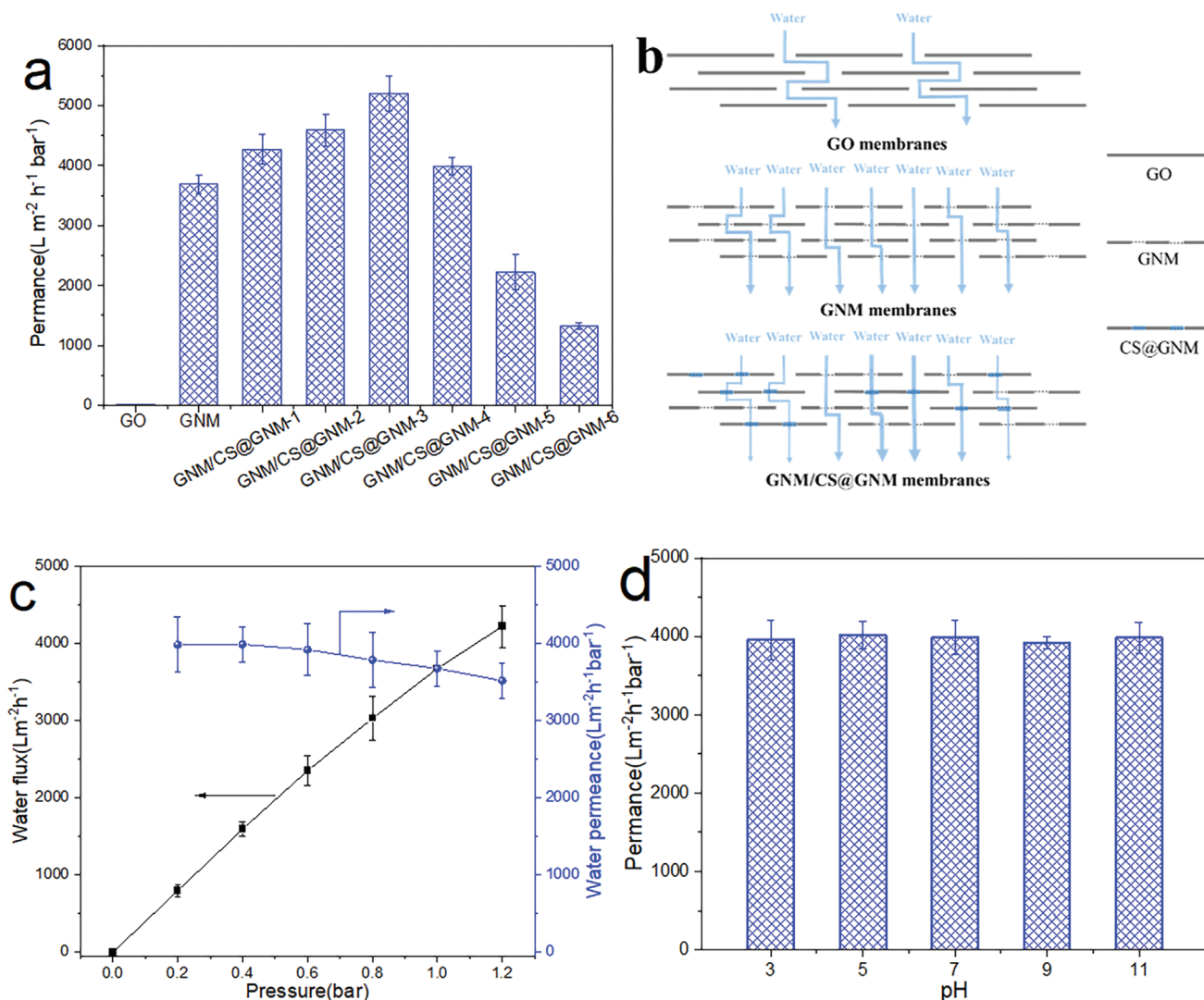


Figure 4. a) Permeance of the cell membrane-inspired GNM membrane, b) schematic diagram of GO membranes, GNM membranes and GNM/CS@GNM membranes, c) water flux and water permeance of the cell membrane-inspired GNM/CS@GNM-4 membrane under different transmembrane pressure differences (for pH = 7.0), and d) at different pH under transmembrane pressure difference of 0.4 bar. Each membrane was tested at least three times.

The morphological stability of the cell membrane-inspired GNM membrane was evaluated through testing the permeance of the membranes under different transmembrane pres-

ures, and using water of different pH. The structural stability after immersion in water for a long time was also tested. The water flux of the cell membrane-inspired GNM membrane

Table 1. Thickness, permeance, water contact angle, time for the water contact angle to drop to zero, and oil contact angle underwater of the GO, GNM and cell membrane-inspired CS@GNM membranes.

Membrane	Thickness [nm]	Permeance [L m ⁻² h ⁻¹ bar ⁻¹]	Water contact angle [°]	Time [s]	Oil contact angle underwater [°]
GO	35.7 ± 6.0	16 ± 2	83.1 ± 4.0	–	143.7 ± 2.3
GNM	42.8 ± 5.3	3690 ± 160	105.5 ± 5.0	16.3 ± 3.2	110.7 ± 3.4
GNM/CS@GNM-1	49.0 ± 6.1	4270 ± 250	97.5 ± 4.0	30.3 ± 2.8	127.6 ± 3.1
GNM/CS@GNM-2	56.4 ± 8.0	4590 ± 260	89.7 ± 4.6	37.3 ± 3.2	137.6 ± 2.9
GNM/CS@GNM-3	62.2 ± 7.8	5200 ± 300	85.7 ± 3.5	26.2 ± 1.7	143.7 ± 3.5
GNM/CS@GNM-4	67.4 ± 6.7	3990 ± 150	79.7 ± 2.8	22.2 ± 3.5	155.7 ± 2.1
GNM/CS@GNM-5	71.3 ± 8.3	2220 ± 420	77.9 ± 2.8	19.2 ± 3.8	157.2 ± 2.9
GNM/CS@GNM-6	80.2 ± 4.3	1330 ± 460	75.2 ± 3.1	17.6 ± 3.4	159.8 ± 2.6

increased as a function of transmembrane pressure in the range from 0–1.2 bar. The water permeance decreased slightly with transmembrane pressure, which is different from what is observed with GO-based membranes made by intercalating nanomaterials between adjacent GO nanosheets to improve permeance. As the enhanced permeance of such GO-based membranes made by intercalating nanomaterials between adjacent GO nanosheets is realized through enlarging the interlayer spacing, this enlarged interlayer spacing could be easily compressed with increasing transmembrane pressure, leading to a sharp decrease in water permeance.^[21] For the cell membrane-inspired GNM membrane, the enhanced permeance is achieved through nanopores on GNM, which increase the number of mass transfer channels and decrease the length of the mass transfer channels. Hence, the impact of the transmembrane pressure on the permeance is very small. Moreover, the cell membrane-inspired GNM membrane showed a stable permeance in the pH range from 3.0 to 11.0, certifying that the membrane morphology could guarantee stable operation in this pH range. Simultaneously, the swelling resistance of the cell membrane-inspired GNM membrane was tested by immersing the membrane in water for 4 months. For GO-based membranes, the π - π interactions between GO nanosheets could be weakened during immersion in water, leading to swelling of the membrane structure, which could produce a loss in membrane performance and damage of the membranes structure.^[34] For our cell membrane-inspired GNM membrane, the interactions between the carboxyl groups on the GNM and the amino groups on CS@GNM could link the GNM and CS@GNM together to impede the swelling and maintain an intact membrane structure. Accordingly, after immersion in water for 4 months, the cell membrane-inspired GNM membrane's structure remained the same. In contrast, the GO membrane presented obvious damage after immersion in water for 4 months, as shown in Figure S5 (Supporting Information). Meanwhile, after immersion in water for 4 months, there was no obvious change in permeance, which was $4010 \pm 240 \text{ L m}^{-2} \text{ h}^{-1} \text{ bar}^{-1}$ for GNM/CS@GNM-4. Also, the oil droplets were fully rejected when this membrane was used to filtrate surfactant-stabilized oil-in-water emulsions. In addition, there was no observable structural change for the cell membrane-inspired GNM membrane after filtration (Figure S6, Supporting Information). All these results show that our cell membrane-inspired GNM membrane is endowed with high morphological stability.

2.5. Antifouling Property of the Cell Membrane-Inspired GNM Membrane

The antifouling property of the cell membrane-inspired GNM membrane was evaluated through filtering a series of surfactant-stabilized oil-in-water emulsions, prepared from sunflower oil, pump oil, octane, and silicone oil. A transmembrane pressure difference of 0.4 bar was utilized to carry out the oil/water separation process with a near surface stirring speed of 300 rpm. The rejection ratio of oil droplets for the cell membrane-inspired GNM membrane was obtained by UV-spectrophotometry and optical microscopy (Figures S7 and S8, Supporting Information). The results showed that there were

no oil droplets in the filtrate, demonstrating that the oil droplets could be totally rejected by the cell membrane-inspired GNM membrane. **Figure 5** shows the permeance of deionized water (P_{water}), emulsion (P_{emulsion}), and the permeance of deionized water (P_{recovery}) after rinsing with water for 20 min. The hydrophilicity of the cell membrane-inspired GNM membrane was increased with higher fractions of CS@GNM in the membrane, leading to a robust hydration layer on the membrane surface during the separation process. As a result, the water recovery ratio ($\text{FRR} = P_{\text{recovery}}/P_{\text{water}}$) was improved, thus facilitating the excellent antifouling properties. Accordingly, the water recovery ratio rose from 29.9% for the GO membrane to 98.7% for the GNM/CS@GNM-4 membrane during the separation of surfactant-stabilized sunflower oil-in-water emulsion with a water permeance of $3990 \pm 150 \text{ L m}^{-2} \text{ h}^{-1} \text{ bar}^{-1}$, which was more than 260 times that obtained with the GO membrane. At the same time, the cell membrane-inspired GNM membrane possessed excellent antifouling properties for separating other kinds of oil-in-water emulsions, and the water recovery ratio could be maintained to above 96.7% in all cases. Also, the long-term separation performance of the cell membrane-inspired GNM membrane was verified through a cyclic experiment using surfactant-stabilized sunflower oil-in-water emulsion as the model foulant. After three cycles, the water recovery ratio could still remain above 95.2%. All these results prove that our cell membrane-inspired GNM membrane exhibits superior properties for the durable separation of surfactant-stabilized oil-in-water emulsions. A comparison of the antifouling performance with state-of-the-art graphene-based membranes for oil/water separations in the literature is shown in **Table 2**. Our cell membrane-inspired GNM membrane combines superior antifouling with high permeance. Although even better performance was obtained with GO/g-C₃N₄@TiO₂, additional light was required to improve the antifouling properties through photocatalytic degradation of the oil droplets, while no light is needed here.

3. Conclusion

Inspired by the structure of the cell membrane, including aquaporins for fast water transport and hydrophilic polymer brushes on the membrane surface for antifouling properties, chitosan-functionalized graphene nanomesh membranes (GNM/CS@GNM-*x*) were synthesized by a vacuum-assisted self-assembly process. Graphene nanomesh was synthesized by creating nanopores on GO nanosheets to increase the number of mass transfer channels and decrease their length. Combined with the low friction between graphene sheets and water, fast water transport was achieved, reaching up to around $4000 \text{ L m}^{-2} \text{ h}^{-1} \text{ bar}^{-1}$. Chitosan was utilized to modify the GNM to improve its hydrophilicity, leading to a robust hydration layer on the membrane surface. Accordingly, the cell membrane-inspired GNM membranes, GNM/CS@GNM-*x*, exhibited high hydrophilicity, super-oleophobicity and low oil adhesion underwater. During the separation of various surfactant-stabilized oil-in-water emulsions, the membranes presented superior antifouling properties, including a high water flux recovery ratio of more than 96.7% for various kinds of emulsions, staying above 95.2% after three cycles.

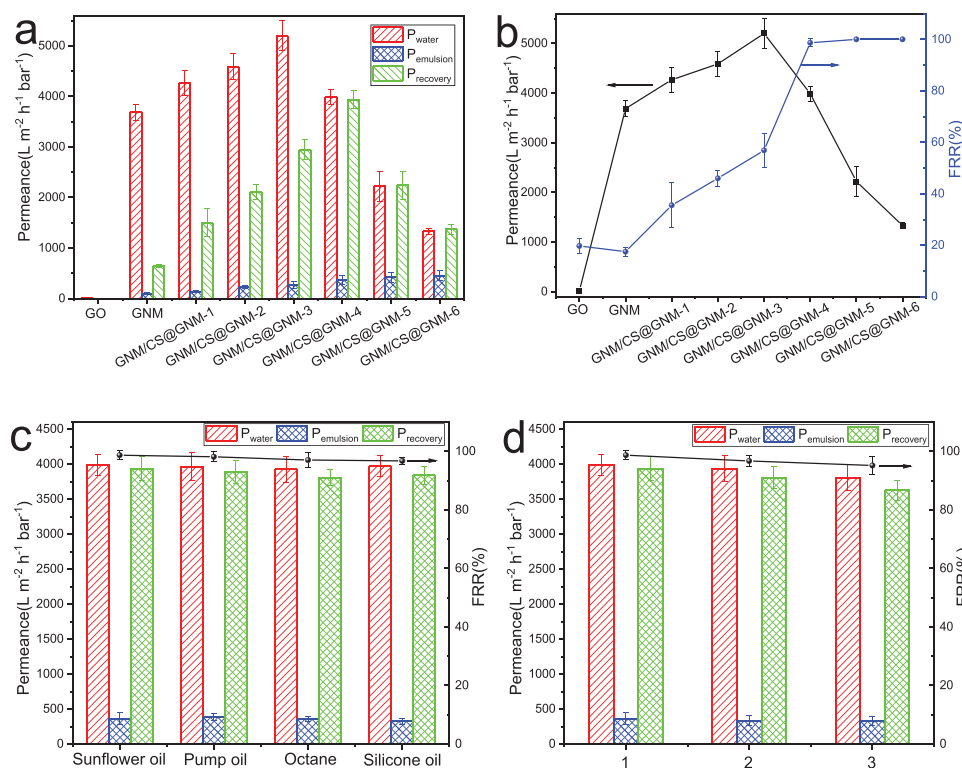


Figure 5. a) The permeance of water, emulsion, and water after recovery for $\Delta p = 0.4$ bar, b) water flux and water flux recovery ratio (FRR), c) permeance of the membranes in water-emulsion-water three-stage filtration experiments for different surfactant-stabilized oil-in-water emulsions, and d) cyclic separation experiments with sunflower oil-in-water emulsion. Each membrane was tested at least three times.

This work provides new insights to fabricate high-performance membranes for oil/water separations through inspiration from nature. Our approach puts a systematic nature-inspired solution methodology to practice that has been developed for a broad range of chemical engineering problems (catalysis, scalable fluid mixing, reaction engineering, fuel cells, membrane separations, etc.) over the past two decades^[54] and is summarized for this example in **Figure 6**. Recently, it has similarly allowed us to realize antifouling microfiltration membranes for tertiary water treatment, where chitosan significantly decreased bio-adsorption of *Escherichia coli*.^[55] Such a systematic nature-inspired solution method does not imitate biology superficially or attempt to cover all the intricacies of cell membranes out of context; instead, it abstracts some of the fundamental physicochemical mechanisms underpinning desired

properties in biological membranes, then implements these specific nature-inspired concepts in designs that use novel materials and manufacturing methods in their implementation. Extending this approach, further progress for a range of other difficult and practically relevant membrane separations could be expected.

4. Experimental Section

Materials: GO nanosheets used in this study were purchased from XF Nano, Inc., China. The nanosheets have an average size of 7 μm and are 0.8 nm thick. $\text{Zn}(\text{NO}_3)_2$ with a purity of 98% was obtained from VWR international Ltd. Chitosan with a molecular weight of 50000–190 000 Da and a deacetylation degree of 76% was supplied by Sigma-Aldrich (UK). HCl with a concentration of 1 mol L^{-1} and glacial acetic

Table 2. Comparison of the antifouling performance with state-of-the-art graphene-based membranes for oil/water separation in the literature.

Membrane	Materials	Permeance [$\text{L m}^{-2} \text{h}^{-1} \text{bar}^{-1}$]	Emulsion types	FRR [%]	Ref.
GNM/CS@GNM	Graphene nanomesh	3989	Surfactant-stabilized oil-in-water	98.7	This work
GO/g- C_3N_4 @ TiO_2	g- C_3N_4 @ TiO_2	4536	Surfactant-stabilized oil-in-water	99.9	[21]
GO/v-COF@GO	v-COF@GO	11 800	Surfactant-stabilized oil-in-water	94.0	[22]
GO/palygorskite	Palygorskite	3866	Surfactant-stabilized oil-in-water	93.0	[49]
PDA/RGO/HNTs	PDA+HNTs	120	Surfactant-stabilized oil-in-water	90.9	[50]
GO/PEG aerogel	PEG	48 900	Surfactant-stabilized oil-in-water	95.6	[51]
GO/APAN	Aminated PAN	10 402	Surfactant-free oil-in-water	67.9	[52]
Graphene/bentonite	Bentonite	625	Surfactant-free oil-in-water	96.0	[53]

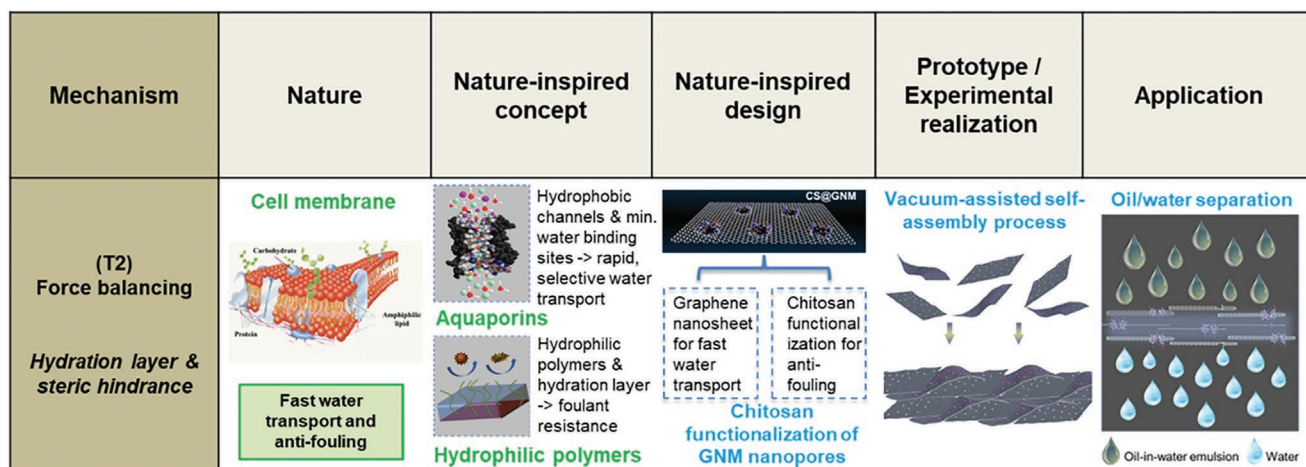


Figure 6. Nature-inspired force balancing mechanisms are used to realize selective high-flux, anti-fouling membranes, as in cell membranes.

acid ($\geq 99.0\%$) were bought from Alfa Aesar (UK) and Honeywell Fluka (UK), respectively. Polyether sulfone (PES) membranes with a pore size of 100 nm were purchased from VWR international Ltd. Deionized water, purified using a Milli-Q system, was utilized throughout all experiments.

Fabrication and Modification of GNM: Nanopores were fabricated on GO nanosheets following a procedure discussed in the literature to produce GNM,^[46] which is included in the Supporting Information. Subsequently, 100 mg chitosan was dissolved in 40 mL water with the help of glacial acetic acid. Then, the obtained GNM was dispersed in the chitosan solution by ultrasonic treatment for 30 min. The solution including GNM and chitosan was kept stirring at 60 °C for 6 h. Chitosan modified GNM (CS@GNM) was collected by centrifugation for 20 min at 6000 rpm and washed three times with water to remove residual chitosan. After that, CS@GNM was obtained by freeze drying for 8 h.

Fabrication of the Cell Membrane-Inspired GNM Membrane: A vacuum-assisted self-assembly process was utilized to fabricate the cell membrane-inspired GNM membrane. GO nanosheets, GNM and CS@GNM were dispersed in water at a concentration of 0.1 mg L⁻¹, respectively (the concentration was calculated using the mass of GNM in CS@GNM). 300 mL dispersions of GO, GNM, CS@GNM, and the mixtures of GNM and CS@GNM were treated by ultrasonication for 10 min. They were then vacuum-filtrated onto PES membranes with a pore size of 100 nm to produce GO membrane, GNM membrane and GNM/CS@GNM membranes, respectively. A series of cell membrane-inspired GNM membranes were fabricated by keeping the total mass of GNM and GNM in CS@GNM constant and changing the ratio of GNM to GNM in CS@GNM. The volume ratios of GNM solution to CS@GNM solution were 300:0, 250:50, 200:100, 150:150, 100:200, 50:250, and 0:300 for GNM, GNM/CS@GNM-1, GNM/CS@GNM-2, GNM/CS@GNM-3, GNM/CS@GNM-4, GNM/CS@GNM-5, and GNM/CS@GNM-6, respectively. The cell membrane-inspired GNM membranes were dried at 60 °C for 12 h before testing them.

Membrane Performance: Membrane performance, including permeance and antifouling property of the cell membrane-inspired GNM membranes, was measured by using a dead-end filtration cell with a filtration area of 4.1 cm² and a Millipore Model 8010. A nitrogen gas cylinder and solution reservoir were equipped to provide a driving force and enough feed solution, respectively. Each membrane was measured at least three times to ensure high reproducibility. Firstly, for each membrane, a specific operation pressure was utilized to recompress the membrane with deionized water to reach a stable permeance. The permeance P (L m⁻² h⁻¹ bar⁻¹) was measured with a transmembrane pressure difference of 0.4 bar and calculated by 10 min filtration of deionized water, based on the equation below:

$$P = \frac{V}{A\Delta t\Delta p} \quad (1)$$

where V (L) is the volume of permeated water, A (m²) is the effective membrane area, Δt (h) is the recorded time, and Δp (bar) is the pressure drop. Four kinds of surfactant-stabilized oil-in-water emulsions were prepared to evaluate the antifouling property of the cell membrane-inspired GNM membranes: 1 g sunflower oil, pump oil, octane and silicone oil were added in 1.0 L deionized water, respectively, and then, 0.1 g sodium dodecyl sulfate was used to stabilize the oil to form the surfactant-stabilized oil-in-water emulsions under mechanical stirring for more than 12 h (Figure S9, Supporting Information). Then, a three-stage filtration experiment of water-emulsion-water was carried out to measure the antifouling property of the cell membrane-inspired GNM membranes, including 10 min water filtration (P_{water}), 10 min emulsion filtration (P_{emulsion}) and 10 min water filtration (P_{recovery}) after 20 min water rinsing. The concentrations of oil droplets in the feed solution and filtration solution were measured by a UV-spectrophotometer (Cary 60 UV-vis) and microscope (Zeiss Axio Observer 5). The water recovery ratio ($\text{FRR} = P_{\text{recovery}}/P_{\text{water}}$) was calculated to evaluate the antifouling property of the membranes, and a higher water recovery ratio demonstrated better antifouling properties. Each membrane was tested at least three times to ensure the repeatability of membrane performance.

Characterization: The TEM and AFM images of GNM were acquired by using a JEOL 2100 200 kV, fitted with a LaB6 filament and BRUKER Dimension Icon, respectively. The chemical structures of GO, chitosan, GNM and CS@GNM were evaluated by a Fourier transform infrared spectrometer (FTIR, VERTEX 70, Bruker, UK) with a resolution of 4 cm⁻¹ for each spectrum, and X-ray photoelectron spectroscopy (XPS) on the Kratos Axis Ultra DLD spectrometer using Al K α (1486.6 eV) as the radiation source was utilized to measure the reaction between CS and GNM in CS@GNM. Thermogravimetric analysis (TGA, Perkin Elmer) was carried out with a temperature range of 50–800 °C and at a rate of 5 °C min⁻¹ in an air atmosphere. The morphology of the cell membrane-inspired GNM membrane was obtained by SEM (FEI Nova NanoSEM 430) and AFM with tapping mode. The wettability of the cell membrane-inspired GNM membrane was measured using a contact angle goniometer (JC2000D2 M Contact Angle Meter), providing the water contact angle, oil contact angle underwater, and the adhesion force between an oil droplet and the membrane surface underwater. Each membrane was tested for at least seven different positions.

Statistical Analysis: The data for permeance was obtained by weighing the mass of filtered solution and calculating based on Equation (1). Other data including membrane thickness and contact angle was directly obtained through characterization. The data was presented in the format of mean \pm standard deviation for the permeance, membrane thickness and contact angle. For membrane permeance and membrane thickness, each membrane was tested at least three times to confirm repeatability.

For membrane thickness and contact angle, measurements were taken at seven positions to acquire this data. Excel was utilized for elementary statistical analysis.

Supporting Information

Supporting Information is available from the Wiley Online Library or from the author.

Acknowledgements

The authors would like to thank Dr. Li Cao (King Abdullah University of Science and Technology) for his kind help for the test of the membrane morphology and Miss Jingyuan Guan (Tianjin University) for her kind support for the measurement of contact angles. This work was supported by the EPSRC via “Frontier Engineering” and “Frontier Engineering: Progression” awards (EP/K038656/1, EP/S03305X/1).

Conflict of Interest

The authors declare no conflict of interest.

Data Availability Statement

The data that support the findings of this study are available from the corresponding author upon reasonable request.

Keywords

nature-inspired, graphene nanomeshes, water treatment, antifouling, oil/water separation

Received: January 6, 2022

Revised: March 26, 2022

Published online:

- [1] M. A. Shannon, P. W. Bohn, M. Elimelech, J. G. Georgiadis, B. J. Marinas, A. M. Mayes, *Nature* **2010**, 452, 337.
- [2] Y. Xu, C. Zhang, P. Lu, X. Zhang, L. Zhang, J. Shi, *Nano Energy* **2017**, 38, 494.
- [3] I. Haddeland, J. Heinke, H. Biemans, S. Eisner, M. Flörke, N. Hanasaki, M. Konzmann, F. Ludwig, Y. Masaki, J. Schewe, *Proc. Natl. Acad. Sci. USA* **2014**, 111, 3251.
- [4] J. Ge, H. Y. Zhao, H. W. Zhu, J. Huang, L. A. Shi, S. H. Yu, *Adv. Mater.* **2016**, 28, 10459.
- [5] L. K. Wang, J. P. Chen, Y.-T. Hung, N. K. Shammass, *Membrane and Desalination Technologies*, Vol. 13, Springer, Science+ Business Media, LLC, **2008**.
- [6] Z. Chu, Y. Feng, S. Seeger, *Angew. Chem., Int. Ed.* **2015**, 54, 2328.
- [7] Y. Liu, Y. Su, X. Zhao, R. Zhang, T. Ma, M. He, Z. Jiang, *J. Membr. Sci.* **2016**, 499, 406.
- [8] Y. Liu, Y. Su, X. Zhao, Y. Li, R. Zhang, Z. Jiang, *J. Membr. Sci.* **2015**, 486, 195.
- [9] G. Kwon, A. K. Kota, Y. Li, A. Sohani, J. M. Mabry, A. Tuteja, *Adv. Mater.* **2012**, 24, 3666.
- [10] A. K. Kota, G. Kwon, W. Choi, J. M. Mabry, A. Tuteja, *Nat. Commun.* **2012**, 3, 1025.
- [11] Y. Liu, Y. Su, J. Cao, J. Guan, L. Xu, R. Zhang, M. He, Q. Zhang, L. Fan, Z. Jiang, *Nanoscale* **2017**, 9, 7508.
- [12] S. Park, K.-S. Lee, G. Bozoklu, W. Cai, S. T. Nguyen, R. S. Ruoff, *ACS Nano* **2008**, 2, 572.
- [13] Q. Cheng, J. Duan, Q. Zhang, L. Jiang, *ACS Nano* **2015**, 9, 2231.
- [14] Y. Qian, J. Shang, D. Liu, G. Yang, X. Wang, C. Chen, L. Kou, W. Lei, *J. Am. Chem. Soc.* **2021**, 143, 5080.
- [15] R. Joshi, P. Carbone, F.-C. Wang, V. G. Kravets, Y. Su, I. V. Grigorieva, H. Wu, A. K. Geim, R. R. Nair, *Science* **2014**, 343, 752.
- [16] G. He, M. Xu, J. Zhao, S. Jiang, S. Wang, Z. Li, X. He, T. Huang, M. Cao, H. Wu, M. D. Guiver, Z. Jiang, *Adv. Mater.* **2017**, 29, 1605898.
- [17] K. Liang, E. M. Spiesz, D. T. Schmieden, A.-W. Xu, A. S. Meyer, M.-E. Aubin-Tam, *ACS Nano* **2020**, 14, 14731.
- [18] D. A. Dikin, S. Stankovich, E. J. Zimney, R. D. Piner, G. H. Dommett, G. Evmenenko, S. T. Nguyen, R. S. Ruoff, *Nature* **2007**, 448, 457.
- [19] Y. Wu, C.-F. Fu, Q. Huang, P. Zhang, P. Cui, J. Ran, J. Yang, T. Xu, *ACS Nano* **2021**, 15, 7586.
- [20] K. Guan, Y. Jia, Y. Lin, S. Wang, H. Matsuyama, N. Lett, **2021**, 21, 3495.
- [21] Y. Liu, Y. Su, J. Guan, J. Cao, R. Zhang, M. He, K. Gao, L. Zhou, Z. Jiang, *Adv. Funct. Mater.* **2018**, 28, 1706545.
- [22] Y. Liu, J. Guan, Y. Su, R. Zhang, J. Cao, M. He, J. Yuan, F. Wang, X. You, Z. Jiang, *J. Mater. Chem. A* **2019**, 7, 25458.
- [23] Y. Han, Z. Xu, C. Gao, *Adv. Funct. Mater.* **2013**, 23, 3693.
- [24] A. Alammari, S.-H. Park, C. J. Williams, B. Derby, G. Szekely, *J. Membr. Sci.* **2020**, 603, 118007.
- [25] J. Guan, X. You, B. Shi, Y. Liu, J. Yuan, C. Yang, X. Pang, H. Wu, J. Shen, C. Fan, *J. Membr. Sci.* **2021**, 638, 119706.
- [26] J. Abraham, K. S. Vasu, C. D. Williams, K. Gopinadhan, Y. Su, C. T. Cherian, J. Dix, E. Prestat, S. J. Haigh, I. V. Grigorieva, *Nat. Nanotechnol.* **2017**, 12, 546.
- [27] W. Li, W. Wu, Z. Li, *ACS Nano* **2018**, 12, 9309.
- [28] J. Yang, D. Gong, G. Li, G. Zeng, Q. Wang, Y. Zhang, G. Liu, P. Wu, E. Vovk, Z. Peng, *Adv. Mater.* **2018**, 30, 1705775.
- [29] K. Guan, S. Wang, Y. Ji, Y. Jia, L. Zhang, K. Ushio, Y. Lin, W. Jin, H. Matsuyama, *J. Mater. Chem. A* **2020**, 8, 25880.
- [30] H. Ma, X. Chen, S. Mohammed, Y. Hu, J. Lu, G. P. Simon, H. Hou, H. Wang, *J. Mater. Chem. A* **2020**, 8, 25951.
- [31] J. Guo, H. Bao, Y. Zhang, X. Shen, J.-K. Kim, J. Ma, L. Shao, *J. Membr. Sci.* **2021**, 619, 118791.
- [32] G. He, M. Xu, J. Zhao, S. Jiang, S. Wang, Z. Li, X. He, T. Huang, M. Cao, H. Wu, *Adv. Mater.* **2017**, 29, 1605898.
- [33] J.-h. Song, H.-W. Yu, M.-H. Ham, I. S. Kim, *Nano Lett.* **2018**, 18, 5506.
- [34] S. Zheng, Q. Tu, J. J. Urban, S. Li, B. Mi, *ACS Nano* **2017**, 11, 6440.
- [35] H. Liu, H. Wang, X. Zhang, *Adv. Mater.* **2015**, 27, 249.
- [36] L. Chen, G. S. Shi, J. Shen, B. Q. Peng, B. W. Zhang, Y. Z. Wang, F. G. Bian, J. J. Wang, D. Y. Li, Z. Qian, G. Xu, G. P. Liu, J. R. Zeng, L. J. Zhang, Y. Z. Yang, G. Q. Zhou, M. H. Wu, W. Q. Jin, J. Y. Li, H. P. Fang, *Nature* **2017**, 550, 415.
- [37] V. Saraswat, R. M. Jacobberger, J. S. Ostrander, C. L. Hummell, A. J. Way, J. Wang, M. T. Zanni, M. S. Arnold, *ACS Nano* **2018**, 12, 7855.
- [38] H. Huang, Z. Song, N. Wei, L. Shi, Y. Mao, Y. Ying, L. Sun, Z. Xu, X. Peng, *Nat. Commun.* **2013**, 4, 2979.
- [39] G. He, C. Chang, M. Xu, S. Hu, L. Li, J. Zhao, Z. Li, Z. Li, Y. Yin, M. Gang, *Adv. Funct. Mater.* **2015**, 25, 7502.
- [40] B. Mi, *Science* **2014**, 343, 740.
- [41] P. L. Yèagle, *FASEB J.* **1989**, 3, 1833.
- [42] K. Murata, K. Mitsuoka, T. Hirai, T. Walz, P. Agre, J. B. Heymann, A. Engel, Y. Fujiyoshi, *Nature* **2000**, 407, 599.
- [43] C. S. Lee, M. k. Choi, Y. Y. Hwang, H. Kim, M. K. Kim, Y. J. Lee, *Adv. Mater.* **2018**, 30, 1705944.

- [44] J. Bai, X. Zhong, S. Jiang, Y. Huang, X. Duan, *Nat. Nanotechnol.* **2010**, *5*, 190.
- [45] J. Yang, M. Ma, L. Li, Y. Zhang, W. Huang, X. Dong, *Nanoscale* **2014**, *6*, 13301.
- [46] Z. Li, X. Zhang, H. Tan, W. Qi, L. Wang, M. C. Ali, H. Zhang, J. Chen, P. Hu, C. Fan, *Adv. Funct. Mater.* **2018**, *28*, 1805026.
- [47] X.-H. Li, J.-S. Chen, X. Wang, J. Sun, M. Antonietti, *J. Am. Chem. Soc.* **2011**, *133*, 8074.
- [48] Z. Shi, W. Zhang, F. Zhang, X. Liu, D. Wang, J. Jin, L. Jiang, *Adv. Mater.* **2013**, *25*, 2422.
- [49] X. Zhao, Y. Su, Y. Liu, Y. Lip, Z. Jiang, *ACS Appl. Mater. Interfaces* **2016**, *8*, 8247.
- [50] Y. Liu, W. Tu, M. Chen, L. Ma, B. Yang, Q. Liang, Y. Chen, *Chem. Eng. J.* **2018**, *336*, 263.
- [51] M. He, R. Zhang, K. Zhang, Y. Liu, Y. Su, Z. Jiang, *J. Mater. Chem. A* **2019**, *7*, 11468.
- [52] J. Zhang, Q. Xue, X. Pan, Y. Jin, W. Lu, D. Ding, Q. Guo, *Chem. Eng. J.* **2017**, *307*, 643.
- [53] P. S. Dhumal, R. V. Khose, P. H. Wadekar, K. D. Lokhande, S. Some, *Sep. Purif. Technol.* **2021**, *266*, 118569.
- [54] M.-O. Coppens, *Annu. Rev. Chem. Biomol. Eng.* **2021**, *12*, 187.
- [55] J. Li, Y. Liu, L. C. Campos, M.-O. Coppens, *Sci. Total Environ.* **2021**, *751*, 141777.